This is a peer-reviewed, accepted author manuscript of the following article: Loukas, C., Williams, V., Jones, R., Vasilev, M., MacLeod, C. N., Dobie, G., Sibson, J., Pierce, G., & Gachagan, A. (2021). A cost-function driven adaptive welding framework for multi-pass robotic welding. *Journal of Manufacturing Processes*, *67*, 545-561.
https://doi.org/10.1016/j.jmapro.2021.05.004

A Cost-Function Driven Adaptive Welding Framework for Multi-Pass Robotic Welding

Names: Charalampos Loukas[1*], Veronica Williams[2], Richard Jones[2], Momchil Vasilev[1], Charles N. MacLeod[1], Gordon Dobie[1], Jim Sibson[2], Stephen G. Pierce[1] and Anthony Gachagan[1]

[1] *Centre for Ultrasonic Engineering (CUE), Department of Electronic & Electrical Engineering, University of Strathclyde, Glasgow G1 1XQ, UK*

[2]*Babcock International Group*

Devonport Royal Dockyard, Plymouth, Devon, PL1 4SG

*Corresponding author's email: charalampos.loukas@strath.ac.uk

Abstract

Manual teaching of robot paths and welding parameters for multi-pass robotic welding is a cumbersome and time-consuming task, which decreases the flexibility, adaptability, and potential of such systems. This paper introduces and presents a new automated weld parameter and pass deposition sequencing framework, which builds on the current state of the art developments and enables automatic planning of multi-pass welding for single-sided V-groove geometries. By integrating a novel cost-function concept that permutates and identifies the welding parameters for each layer through a user-driven weighting, the framework delivers the minimum number of passes, filler material and welding arc time based on application requirements. A mathematical model relating the cross-section area of beads with the pose of the torch and weaving width was built upon to allow full-process automated welding parameter generation and adaption for different geometric characteristics of the groove. The concept methodology and framework were then developed and verified experimentally, through robotically deployed Metal Active Gas (MAG) welding. For a given representative joint, the arc welding time and amount of filler wire were found to be 32.9% and 26.18% lower respectively, than the worst-case available welding parameter combination, delivering a corresponding decrease in direct automated welding manufacturing costs. Lastly, an ultrasonic inspection was undertaken to verify the consistent quality of the weldments validating the framework outcome and enabling welding pass automation through robotic systems.

Keywords: Robotic Arc Welding, Multi-pass, Weld Sequence Planning, V-groove, MAG

1. Introduction

The need to automate processes in manufacturing lies in the desire for high productivity, reduction of production costs and increase of profits through reduced labour cost [1]. Fusion welding is the process of joining two materials together, typically employing heat through solidification with or without the use of filler consumable material. Over the past decades, welding has made a considerable impact in different sectors of our world including, aviation, automotive, defence and marine through the fabrication of tanks, frigates and submarines [2].

1.1. Arc Welding Technology and Joint Designs

Among the different types of welding, arc welding has evolved for over 100 years [3]. The different types of arc welding can be categorized based on the electrode method used, which is consumable or non-consumable [4]. Among the most common techniques, Gas Metal Arc Welding (GMAW) widely known as Metal Inert Gas (MIG) and Metal Active Gas (MAG) utilize a consumable filler wire. The distinction originates from the shielding gas that is employed, and this technique is suitable for both thin and thick sections resulting in high deposition rates and increased productivity [3–5]. The power source of these welders can be synergically controlled for a given wire material and diameter and in absolute wire feed speed or current mode, depending on which parameter the welder will control. A different variety of metals can be welded, which range from carbon steels, low alloy steels, stainless steels, aluminium alloys, copper, and nickel alloys.

In welded structures, loads are distributed between the welds of the joints. The type of joint geometry is determined through the geometric requirements of the assembly and the type of loading [4]. As can be seen in Figure 1 [6], the basic joint designs are summarized as butt, corner, edge, lap and tee joints. The selection of the joint type also aligns with the requirement for the least amount of deposited weld metal to meet the strength requirements for load distribution [4]. For thick butt joints, the edges are mechanically prepared (machined, water-jet cutting etc.) to a particular geometry to provide adequate access for the weld torch and achieve even heat input flow and penetration between filler and parent metal [3,4]. These mechanically prepared geometries, which are shown in Figure 2 [4], can be single sided or double sided for example with double V's, and single or double U's.

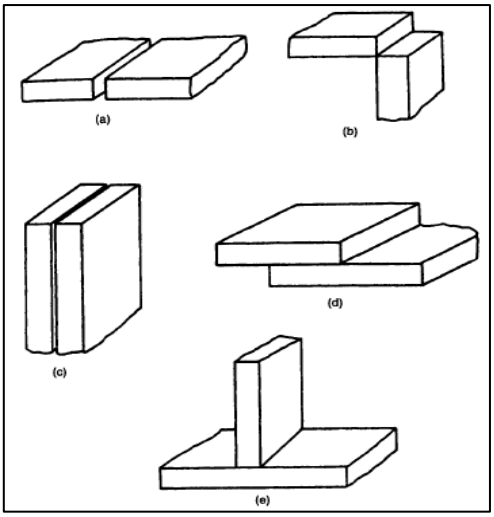

Figure 1. Five basic types of weld joint geometries. (a) butt joint, (b) corner joint, (c) edge joint, (d) lap joint and (e) tee joint

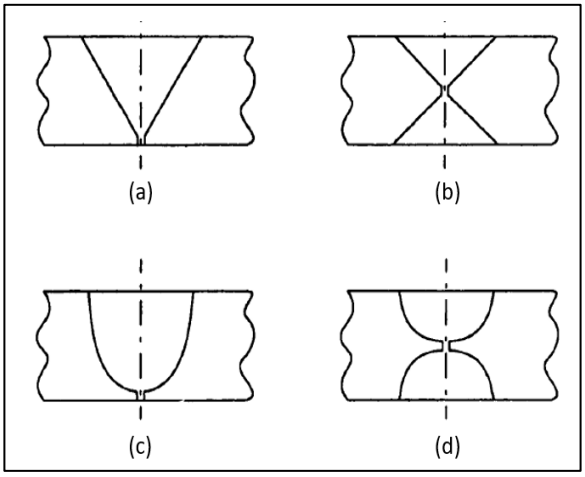

Figure 2. Butt joint geometries processed for welding. (a) single sided -V, (b) double -V, (c) single-U, (d) double-U

61

62 ## *1.2. Multi-Pass Welding Notation*

63 In the maritime, oil and offshore industries, the thickness of the single or double V-groove
64 joints requires more than a single pass, usually manually or semi-autonomously deposited,
65 resulting in low efficiency and productivity [7]. Although manual welding allows selecting
66 different welding parameters per layer or even per pass if that is required, this depends on the
67 experience of the welder and the limits and window of the approved Welding Procedure
68 Specification (WPS) produced from a weld procedure qualification record.

69 Figure 3 describes the terminology of multi-pass welding for a single sided V-groove open root
70 gap assembly. The root pass refers to the initial welding pass used to join parent metals
71 together, where a non-metallic backing strip can be used to support the root surface [3]. The
72 hot pass is the second welding pass used to reshape the root pass, achieve sidewall fusion and
73 fill any inconsistencies caused by improper penetration of the root pass [8]. Filler passes serve
74 the remaining weld groove area until the cap passes are deposited to reinforce the weld groove

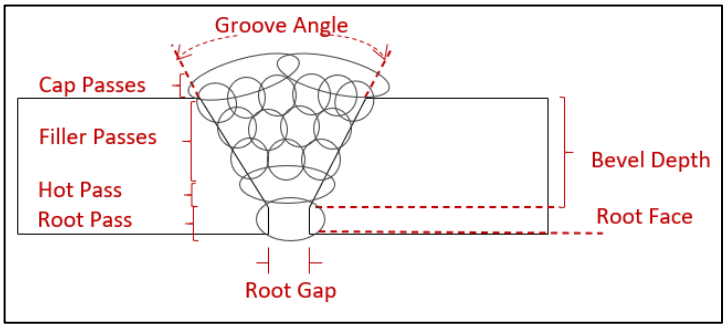

Figure 3. V-Groove joint characteristics and passes notation

and provide a clean finish to the top weld face. Welding passes deposited at the same height offset relative to the root face belong to the same layer. The vertical root face is used for to achieve proper fusion with the root sides.

1.3. Welding Environment and Challenges

Despite the massive utilisation of welding technology in manufacturing, the welding environment still imposes difficulties for the welders. During welding, high concentrations of fumes, gases, dust, infra-red and ultra-violet radiation are produced along with substances, such as nickel and chromium, which have an adverse effect in the human respiratory system and can lead to lung cancer and asthma [9].

Lack of space during welding can amplify the exposure to toxic fumes and increase the ambient temperature. Those unpleasant conditions can be met in enclosed spaces, as it happens in the pre-fabrication of double hull structures [10]. Nonetheless, during the maintenance of such structures, there is limited space for work. Fixed infrastructure that cannot be moved and other manufacturing processes taking place in parallel also increases the possibilities for injuries while working in a confined area.

1.4. Welding Automation

A complex dynamic process such as welding, which is challenging to parameterize and to control [11–14], must meet the demand for high production rates, precision, and consistent quality. However, labour turnover due to harsh environmental conditions further increase the shortage of skilled welders to fulfil the needs of manufacturing in the 21st century [15], affecting production and consistency of quality. Consequently, the life span of future assets can be reduced, and the amount of rework increased [16]. Automating welding can alleviate issues of repeatability, quality, and increased production demand. The bulk production of repeatable welds in multi-pass welding of known joint geometries can be delivered through robotic welding systems. Therefore, freeing welders to be utilized in more complex and creative tasks where a high degree of customisation is required.

When considering automated welding deployment, based on the Degrees of Freedom (DoF) that the welding systems exhibit, these can be commonly classified into either rectilinear (Figure 4(a)-[17]) or articulated robotic solutions (Figure 4(b)-[18]) [19]. Rectilinear robots (gantry systems) can demonstrate a constrained boxed working envelope, moving multiple axes to allow flexibility and volume coverage. Alternatively, articulated robots mimic human arms

106 with six DoF, utilizing revolving wrists connected through joints and controlled by motors to
107 cover the working volume with flexibility and speed.

108 These articulated robotic manipulators exploit interest for specific automation applications, due
109 to their capabilities and multiple DoFs, increased pose repeatability and duty cycles. However,
110 the realisation of fully automated robotic arc welding systems is not yet achieved, as the
111 welding procedure, operating environment, welding joint geometry and preparation can vary
112 significantly [20].

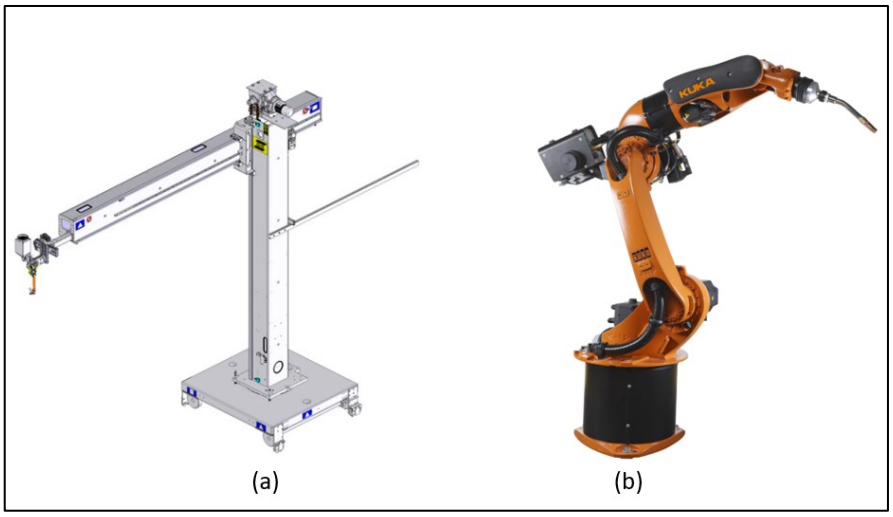

Figure 4. Welding robotic systems classified based on the degrees of freedom (a) Rectilinear robotic system and (b) Articulated robotic arm

113 ### *1.5. Automated Robotic Welding*

114 Considering this progress, and the conditions of common industrial welding environments, the
115 call for flexible automated arc welding can be realized through decisional autonomy [21]. A
116 closed-loop robotic system can alter the trajectory of the motion based on sensory feedback
117 information (camera, laser scanner, touch-sensing). In that way, it can sense the local
118 environment and superposes pre-programmed moves adapting to changes encountered in the
119 environment.

120 The realization of a fully automated robotic welding system demands the development of a
121 welding framework which combines sensor-driven robotic motion along with multi-pass
122 sequence planning for the weld joint geometry. Sequence planning of multi-pass welding is
123 imperative for automation of welding in the shipbuilding and offshore sector due to the
124 requirement of the thickness of the joints. Moreover, this welding process is repetitive and
125 monotonous, while manual welders can be utilized in more complex tasks.

This paper presents a new welding framework that enables automatic planning of the complete multi-pass welding sequence with different welding parameters per layer. Moreover, this approach adapts to varying single sided V-groove geometries, without human intervention, populating the number of layers and passes to minimise a desired cost function. These developments are demonstrated alongside a flexible 6-DoF sensor-driven robotic welding system. The rest of this paper is organised as follows. Section 2 introduces a multi-pass welding sequence review for V-groove joint configurations. Section 3 presents the welding framework and the developed algorithms for automated multi-pass weld planning based on the minimization of a cost function. Section 4 demonstrates the experimental setup, utilizing different butt joint geometries for a proof-of-concept validation along with inspection of the completed joints. The subsequent proof-of-concept demonstration characterization results are discussed in Section 5. Section 6 discusses future work with Section 7 concluding the paper.

2. Automated Multi-Pass Welding

2.1. The Current State-of-The-Art in Multi-Pass Sequence Planning

Mathematically describing and approximating the shape geometry of the deposited welding beads requires developing algorithms to generate the sequence of welding parameters and as a result, the robotic motion path. In the relevant works, welding beads are represented as parallelograms and trapeziums since often the cross-section shapes of weld beads match these shapes visually. Using the same welding parameters for all the deposited weld beads, the authors in [7,22,23] simplified the welding sequence generation. Adopting the same welding parameters for every welding pass, for all the layers, the method of equal height was used in [7,22]. The method assumed that every layer had the same height, which could be argued as partially true since the width of the groove increases between the bottom and the top surface of the specimen. Similarly, in [23], the welding sequence schedule was generated utilizing the same welding bead for all the filling layers. This assumption was held since the cross-section area of the weld bead remains constant under the same welding parameters, resulting in the equal area method.

The number of passes per layer can be minimised by selecting different welding parameters for every layer, and the groove can be filled faster than using the same weld bead for each weld pass. In [24], authors related the cross-section area of the weld bead with the value of the wire feed speed, robot speed and diameter of the wire. Depending on where the weld bead was deposited in the groove it was approximated as a trapezium or a parallelogram. This method

prompted the user to enter the desired welding parameters per layer and number of passes, and outputted the robot pose trajectory and position of weld bead in the groove to aid automation, while mimicking manual welding approaches. The approximation of weld beads as a parabola is discussed in [25]. The welding schedule algorithm assumed that the width of every weld pass in the same layer remains constant and the bead selected maximizes the occupied cross-section area to result in the minimum number of passes. However, no action is taken on the maximum allowed height of every new welding layer, where the user decides as the groove is filled with passes. This call for user action makes the multi-pass welding sequence planning a semi-automatic procedure. In all the relevant works [7,22–25], the user input is required at multiple stages. In the proposed approach documented herein, the user is asked only once to assign welding parameters. Then they will not be prompted to make decisions, as welding parameters can adapt for varying butt joint configurations. Table 1 depicts the current advancements on the state-of-the-art in multi-pass sequence planning along with their limitations.

Table 1. Relevant works in multi-pass weld sequence planning and limitations

Relevant works	Different welding parameters per layer	Adapting different welding parameters to varying V-groove geometries	Cap passes planning	Post-Trial Inspection Verification
C.D. Yang et al.[7]	✗	✗	✗	✗
C. Yang et al. [22]	✗	✗	✗	✗
T.-Y.Huang et al.[23]	✗	✗	✓	✓
H. Zhang [24]	✓*	✓*	✗	✗
S.J. Yan et al.[25]	✓**	✓**	✗	✗
This Body of work	✓	✓	✓	✓

* The user prompts to enter the welding parameters per layer. In that way, it can select different welding parameters for different V-groove geometries.

**Welding parameters are provided from a bank of parameters where the user decides for the initial number of passes and layer height. The chosen dimensions of the bead must satisfy the stored configurations in the database

2.1.1. Research Gap and Opportunity

The research gap based on prior literature, indicated the lack of an automated technique to identify the combination of the welding parameters per layer and the number of welding layers to fill the V-groove geometries without user intervention. Zhang et al. in [24] prompted the user to decide for the welding parameters per layer, while in [7,22,23] the same welding bead was deployed in every pass of each layer, which is not always efficient in terms of welding time and heat input required. The maximum height and width of the planned passes were not

discussed, and as a result, the chosen weld passes could have an irregular cross-section area relative to the size of the whole groove. Two common points of the above approaches was the use of backing to deposit the root pass, and the fact that the hot pass was treated as a regular filling pass when more heat is required than the first pass to fill any inconsistencies caused by improper penetration of the root pass [8]. Moreover, cap planning and inspection for defects were only performed in [23] where the micrograph analysis revealed a lack of sidewall fusion.

Building and adapting on the work reported in [24] the following advancements and work packages are developed in this body of work, where Figure 5 summarizes and illustrates the developed contribution of the automated multi-pass weld sequence framework:

- The opportunity from the research gap is realized by developing an algorithm to automate the sequence path planning with different welding parameters per layer and identifying the number of passes per layer and number of layers irrespective of the butt joint geometric characteristics.
- A logic is integrated to allow the adaption of the sequence of welding parameters for varying single sided V-groove geometries (groove angle, gap size, bevel height) enabling the automated robotic weld path planning. This advancement can eliminate additional time to re-program, from scratch, the robot motion when the joint geometry changes due to design or operational requirements.
- Additional work is performed to formalize the need for cap planning in the final welding layer for varying V-groove geometries.
- The optimized solution of the sequence of welding parameters per layer is shaped further by introducing the dynamic concept of the cost function. This delivers the combination of welding parameters that will produce the minimum number of passes in the minimum arc welding time, with the minimum spent filler material while taking care of the restrictions on allowed height and weaving width of the weld bead. The size

of the bead can increase the residual stress between weld passes, leading to cracks and increased distortion of the weldment [26,27].

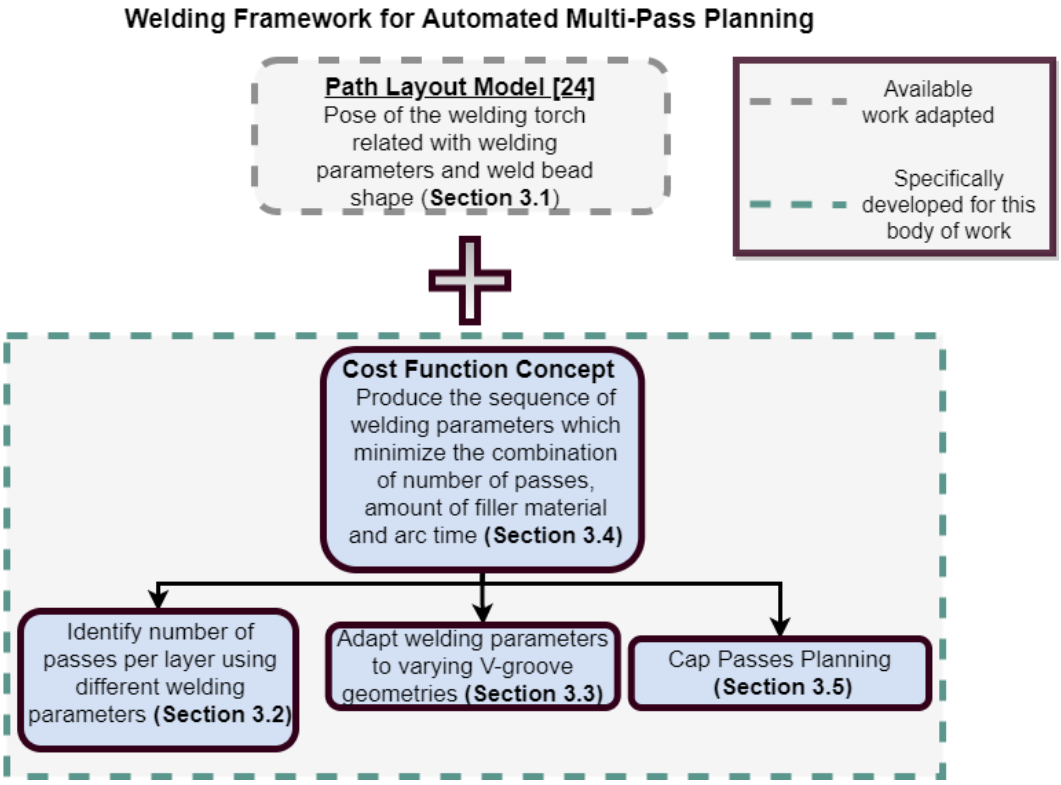

Figure 5. Highlighted is the available adapted and newly developed work for this paper with direct reference to their corresponding section in the paper

3. Proposed Automated Welding Framework

A mathematical model, relating the cross-section area of beads with the welding parameters, pose of the torch and weaving width, was adopted from [24] and built upon to allow full-process automated welding parameter generation, optimization and robotic path planning. The flowchart in Figure 6 describes each step of the welding framework as well as the required user input. The following sections explains in detail the implementation of the different steps along with the notation used in the diagram.

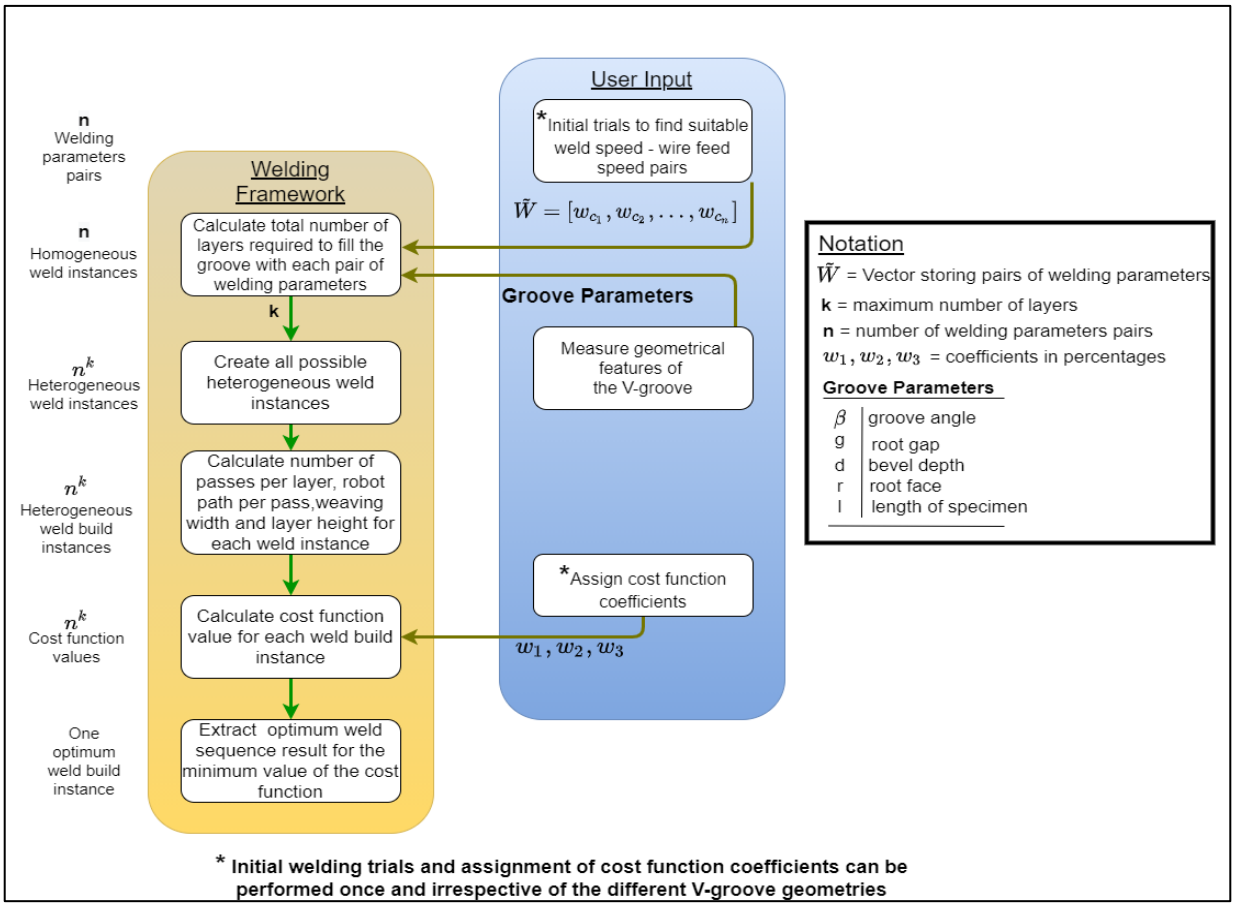

Figure 6. Flowchart presenting the welding framework process and the required user input

222

223 *3.1. Cross-section Area and Efficiency Coefficient*

224 An integral part of the welding framework is the prediction and approximation of the cross-
225 section area of a deposited weld bead based on the welding parameters. The cross-section area
226 defined with variable S (mm^2) is represented by a trapezium or parallelogram shape depending
227 on where it is deposited within the groove [24] and is given by Eq:3:1

$$S = \frac{\pi \cdot u \cdot D^2}{2 \cdot v} \qquad \text{Eq:3:1}$$

228 where u = wire feed speed ($^{mm}/_{s}$), D = diameter of the wire (mm) and v = robot welding
229 speed ($^{mm}/_{s}$). Every pair of robot and wire feed speed is provided as a welding configuration
230 vector, $w_c = [v, u]$. To reflect the material loss during welding, due to the efficiency of the
231 filler wire, spatter and heat transfer, the coefficient a_H was introduced, to give Eq:3:2 based on
232 [7,22]. The coefficient a_H was determined through experiments and subsequent welding trials.

$$S = \frac{a_H \cdot \pi \cdot u \cdot D^2}{4 \cdot v} \qquad \text{Eq:3:2}$$

3.2. Assess the Number of Layers and Passes

The automatic generation of the number of layers and passes required was obtained by building on [24] where the user was prompted to provide the total number of layers and passes. The root and hot pass were not part of this routine, as they each constitute one welding pass. The number of welding passes for every new layer is now automatically calculated based on the parameters shown in Table 2, and driven by restrictions on the maximum weaving width and the range of allowed height of every weld bead on the layer. This is core of the developed algorithm, highlighted in the flowchart of Figure 7 with the green dotted lines.

Table 2. Inputs of the algorithm that produce the number of passes per layer

Parameter	Description
w_c	Generated vector of welding parameters (see Sec. 3.1 above)
S	Array of values of cross-section areas of already deposited weld beads
m_i	Number of already deposited passes per layer
i	Current layer number
a_H	Deposition coefficient (see Sec. 4.2)
δ	Weaving factor used to restrict weaving width (see Sec. 4.2)
β	Groove angle of V-groove
g	Root gap length
D	Diameter of filler wire

The range of accepted height and maximum weaving width of a weld pass are not defined explicitly in welding standards but is guided mainly from the requirements of the application and is recorded as part of the WPS. However, the narrower and taller the bead is, the more challenging it is to perform subsequent weld passes and to achieve proper fusion with the sides of the weld bead. On the other hand, weld beads with a smaller height lead to more passes to fill the remaining groove, which is not efficient in terms of manufacturing time.

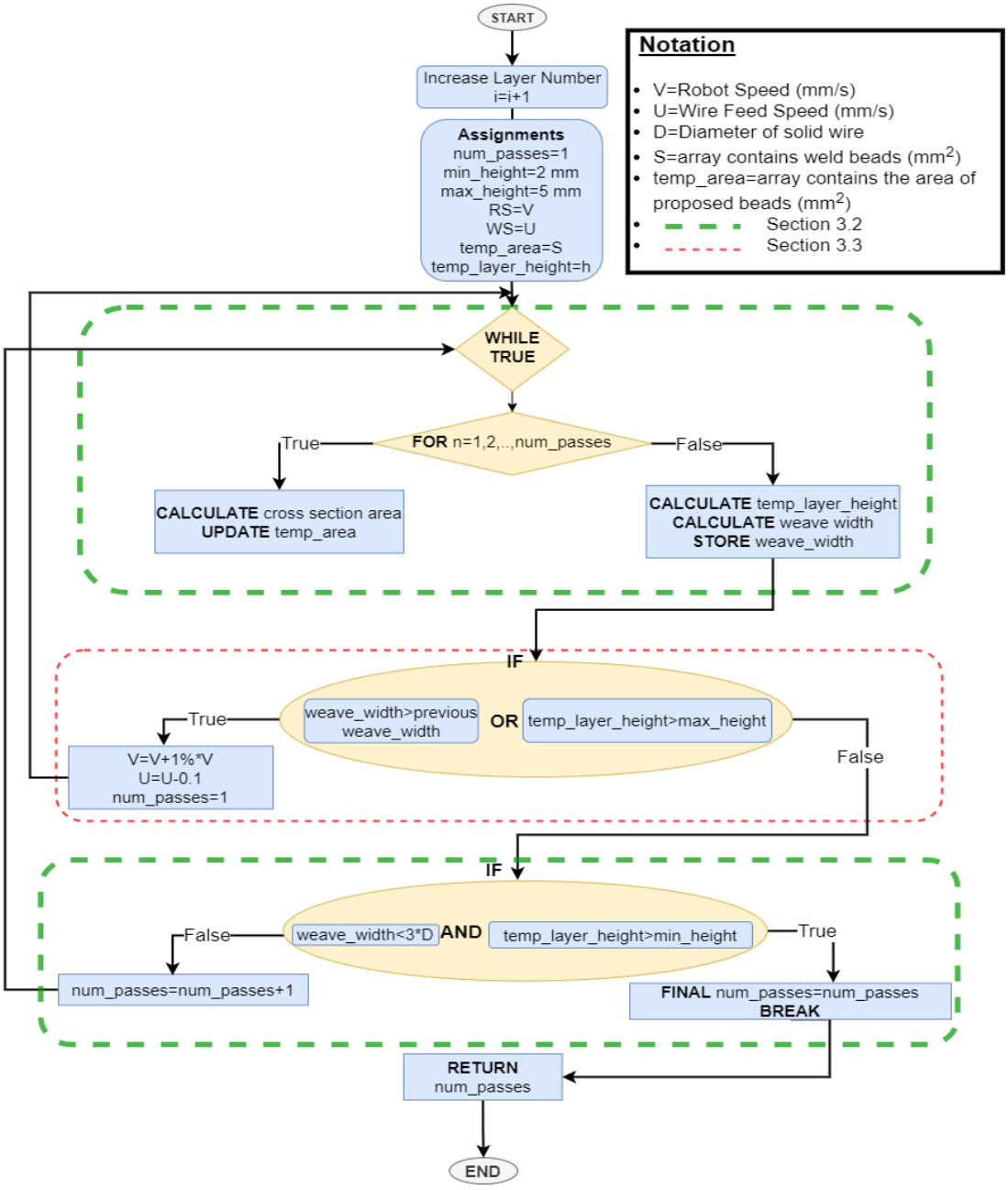

Figure 7. Process flowchart of the developed algorithm. The algorithm also adjusts the welding parameters based on the imposed restrictions of bead height and weave width

Preliminary experimental trials deployed with the robotic setup presented in Section 4 showed that the acceptable range of height of each layer could be between 2 mm and 5 mm. Moreover, the maximum weaving width was limited to three times the diameter of the welding wire ($3 \cdot D$) used. Excessive weave width increases heat input towards inline cracking and the chance for lack of fusion with the sidewalls.

3.3. Adapting Welding Parameters to Varying V-groove Geometries

Lastly, the process marked with red dotted lines in Figure 7, assists in generating the number of passes per layer for varying groove geometries, irrespective of the characteristics of the butt

joint (bevel angle, height, root gap). As operator input is not required for each layer, to guarantee that the restrictions on height and weave width are satisfied, a logic is encapsulated to adapt the given welding parameters.

Investigating the variation on the geometric characteristics on the V-groove joint, there is a possibility that the cross-section areas of the produced welding beads based on the given welding parameters will never satisfy the restrictions on height and weave width of the welding beads. These variations which were validated from experimental procedures consist of a groove angle further of 95º, root gap length more than 2 mm and the total height of 15 mm.

Violating the restrictions, stems from the rise of the width groove from bottom to top and in which height previous deposited layers were within the groove. More particularly equations from [24] were used to calculate the height of the layer and required weaving width of passes. Both depend on the previous layers' height and covered area from already deposited weld beads. For every new layer, the algorithm initially picks a welding parameters pair and assigns one pass which will have large weaving width and very small height to occupy the whole layer. In the next iteration a new pass will be added, so the weaving width will decrease and because more passes stack together the height of the layer will increase. But in some circumstances, by adding more passes in that layer may never satisfy the restrictions as the initial cross section area of the pass was too big and the height of the layer will keep increasing. To counteract this action and always satisfy the imposed size limits the cross-section area formed from the existing welding parameters must decrease. Hence, once there is a violation, the provided welding configurations are adjusted in every iteration, by 1% of the robot speed and 0.1 m/min the wire feed speed. These incremental proportional changes (1%, 0.1 m/min) were selected, as are the minimum allowed increments in the robotic and welder equipment setup used for the experimental proof of concept (Section 4). If larger increments were selected, the restrictions would be satisfied in fewer iterations. Still, the cross-section area of the welding passes would be much different from the welding parameters that the user initialized at the start of the framework and at the end may not be accepted if the deviation is outside of the accepted window of the WPS document. It must be stressed also that large cross-section area beads produced from increased wire feed speed, may fill faster the area and volume of the groove, but will require more iterations to adjust the welding parameters if the restrictions are violated.

3.4. Cost Function and Sequence of Welding Parameters

In manual welding, the sequence of welding parameters per layer is not always known beforehand. Therefore, when considering automated welding**,** the total number of layers, welding passes, arc time and the amount of filler wire material that will be required are often unknown variables in the multi-pass weld planning procedure. As these parameters drive the actual costs of welding, they can be used to form a cost function. Such a cost function can be assigned by the operator and could be minimised, leading to the most optimum welding procedure.

For a given V-groove geometry and a produced sequence of welding parameters, the cost function proposed is the weighting summation of the number of passes, the amount of filler material and total arc time required. It takes the form of Eq:3:3 where w_1, w_2, w_3 are the

$$C(w_1, w_2, w_3) = w_1 \cdot passes + w_2 \cdot material + w_3 \cdot time \qquad \textbf{Eq:3:3}$$

weighting coefficients which must add up to 100% in total. These weighting coefficients are set by the operator, based on which parameter they would like to minimise the most.

The value of number of passes per layer are given from the algorithm described in Section 3.2. Regarding the arc time and amount of filler material per layer is given by Eq:3:4 and Eq:3:5 respectively.

$$Arc\ time/layer = \sum arc\ time/pass$$
$$arc\ time/pass\ = \ Length\ specimen/v \qquad \textbf{Eq:3:4}$$

$$Filler\ material\ /\ layer = \sum material/pass$$
$$material/pass\ = \ (wire\ weight/mm) * length\ of\ wire$$
$$length\ of\ wire = (arc\ time\ /pass) * u \qquad \textbf{Eq:3:5}$$

To automate this process, the user initially defines the welding parameters that will be used in the welding framework providing in pairs of w_c vectors, as mentioned in section 3.1, and are feasible from the welder equipment regarding heat input and welding speed. It must be noted that utilizing beads with increased cross-section area by increasing the wire feed speed u and keeping constant the robot speed v, will result in a decreased number of passes to fill the V-groove volume. However, the welding parameters must be approved from the relevant WPS document regarding the properties of the joint material. Increased wire feed speed and as a result increased current can result to excessive heat input, damaging the internal structure of the material and generating defects.

These welding configurations are stored as a vector $\widetilde{W} = [w_{c_1}, w_{c_2}, \dots, w_{c_n}]$ where $n \in Z^+$ is the length of the vector and shows the number of different welding parameters. The vector $\widetilde{W}$ remains constant for all the varying V-groove geometries that welding is scheduled.

3.4.1. Homogeneous Weld Instances

Firstly, the total number of layers that can fit in a provided V-groove geometry has to be estimated based on the assigned vector $\widetilde{W}$. Following the root and hot pass which are not generated from the developed welding framework, the number of welding layers for the remaining volume of the groove can be found by iterating through $\widetilde{W}$, and creating instances of the same geometry where each layer is assigned the same welding configuration.

This is illustrated in Figure 8, where the generated samples of the V-groove geometry can be seen. The number of passes per layer is found, utilizing the algorithm described in sections 3.2 and 3.3.

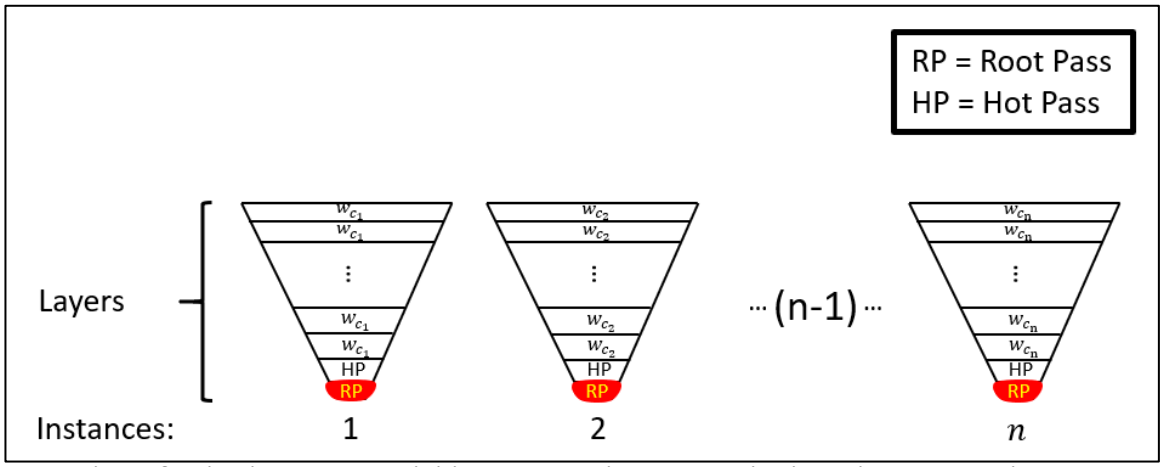

Figure 8. Highlighted are the initial generated instances which investigate the maximum number of layers that fitted among all the n different welding configurations in $\widetilde{W}$ vector

The w_c welding configuration per layer is adjusted if the restrictions of height and weaving criteria are violated. Therefore, n different instances are created for the same geometry and the maximum number of layers that found from this iterative process is recorded and defined as $k \in Z^+$.

3.4.2. Heterogeneous Weld Instances

Permutations within iterations are utilized to determine all the different ways that the welding parameters can be assigned for the maximum number of layers found, while addressing the need for varying welding parameters as the layers are generated. The number of permutations can be found using Eq:3:6, and these are populated schematically in array P of Figure 9.

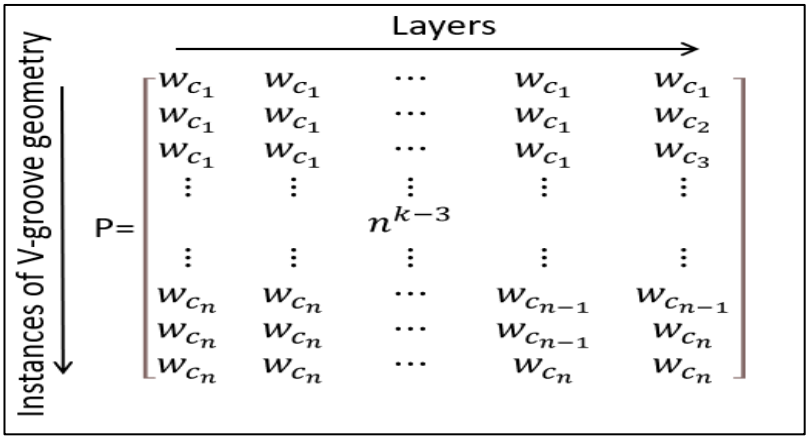

Figure 9. Array P is generated from populating the welding parameters per layer for n different welding configurations w_c using permutations within iterations

Iteration is used since every new layer can have the ability to get assigned the same welding configuration w_c as the previous layer.

$$\mathrm{P_n^k} = \mathrm{n^k} \text{ where } \mathrm{k, n} \in \mathrm{Z^+} \qquad \textbf{Eq:3:6}$$

For example, if $n = 4$ different welding configurations of w_c, assigned in the framework as vector $\widetilde{W}$ and $k = 6$, found from the process described in Section 3.4.1, then $4^6 = 4096$ different sequences of welding parameters, for the same groove geometry, can be generated, utilizing only four other welding parameters. However, not all the generated welding sequences are unique, since the value k that was found is a rough estimation of how many layers can fit in the V-groove when all the layers have the same welding parameters. The restrictions on height and weaving width that are imposed when a new pass is added to the layer affect the height where every layer will reach within the V-groove. The algorithm reported in [24] that

calculates the weaving width of a pass is guided from the summation of the cross-section areas of previous beads and the height where the last layer reached. Combining this fact with the V-groove shape, where by definition the width of the groove increases from bottom to top and more passes can fit per layer, the number of total layers at the end may not be equal to the estimated value k (see Section 3.4.1). Besides, layers with welding parameters that follow a swapped order result from the permutations (i.e. $[w_{c_1} - w_{c_2} - w_{c_1}]$, $[w_{c_1} - w_{c_1} - w_{c_2}]$,$[w_{c_2} - w_{c_1} - w_{c_1}]$) and have different cross section area, may not reach the same height as they can be deposited in a different height offset from the root face. As a result, the restrictions can generate different number of passes in these instances. The existence of these cases requires one additional layer, and this depends on the sequence of welding parameters that were populated until reaching the formation of these layers. For that reason, permutations within iterations are investigated for $k + 1$ possible welding layers with n pairs w_c of welding configurations to compensate for these cases.

3.4.3. Weld Build Instances and Cost Function Calculation

Populating the array P with dimensions $n^k \times k$, as shown above in Figure 9 which stores the permutations of different welding sequences for a given V-groove geometry, is essential to find all the values of the cost function. A V-groove instance filled by layers is created, where each layer following the root and hot pass, gets assigned the welding parameters per column of the array P. For every generated layer the algorithm analysed in section 3.2, is used to generate the number of passes where the amount of filler wire, the arc welding time and the number of passes is recorded based on Eq:3:4 and Eq:3:5. New layers are added until the top surface of the V-groove is reached and the robotic path per pass is generated based on [24] and welding parameters assigned per layer. Regarding the arc welding time, optional time of 10 seconds should be added after depositing each pass to avoid contamination with following passes. Eq:3:3 is used to calculate the value of the assigned cost function. This process is repeated for all the rows of array P, until n^k weld build instances are populated and those that resulted in the same cost value are rejected.

For example, assuming the annotated geometry in Figure 10, the proposed solution for the sequence of the welding parameters derives from the minimum value of the cost function $C(60\%, 10\%, 30\%)$. Schematics in Figure 10(a), (b) represents the number of layers, along with the generated passes and pose of the weld torch. The values of the cost function for all 1071 generated unique instances highlight the extreme maximum and minimum values and all the

different ways that the geometry can be welded utilizing four different welding configurations w_c. The aim was to minimize the number of passes; thus, the first weighting coefficient was selected to be 60%. Comparing the results from the maximum cost value relative to the

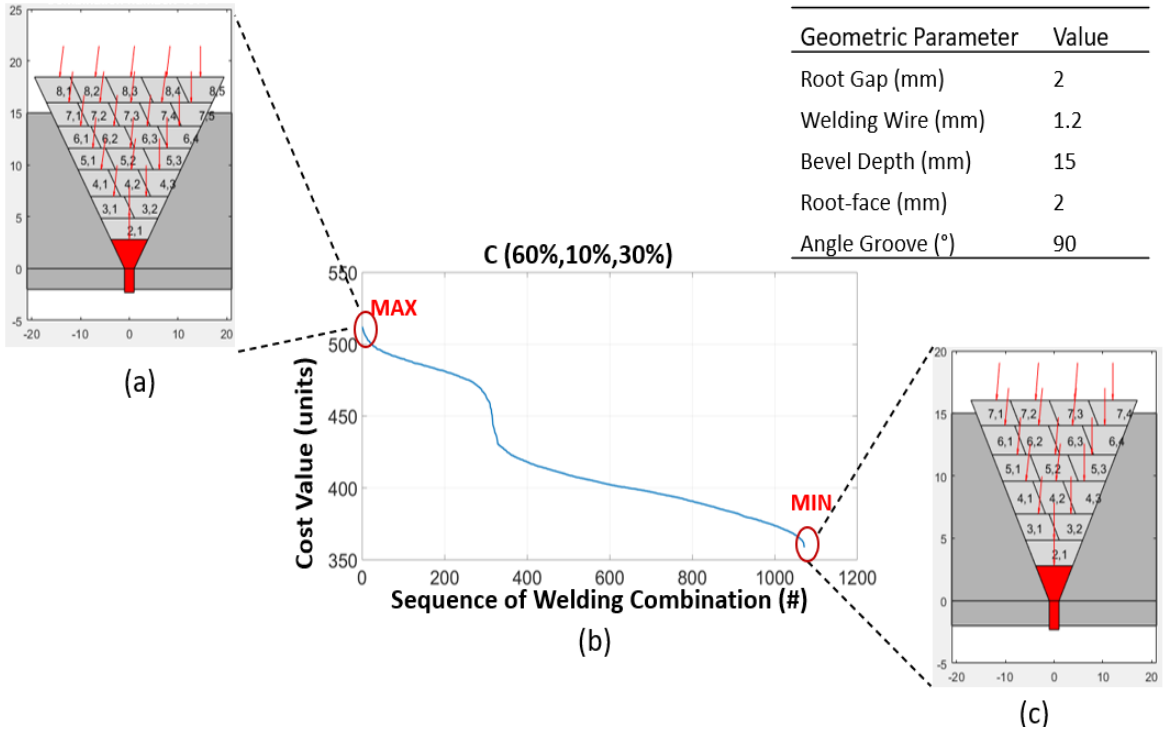

Figure 10. Highlighted cost function built from 1071 unique instances using 4 different welding configurations for 7 possible layers: (a) Solution from maximum cost value showing additional required six passes and increased welding time of 44.49%, (b) Cost function along the sequences of welding combinations, (c) Solution from minimum cost value showing a decrease of 34.24% in filler wire and six welding passes less than the maximum result

minimum requires 6 more passes, the welding time is increased by 44.49% and filler wire is 34.24% higher. This result validates the benefits linked to the cost function concept, which decreases the actual costs of automated welding, through reduced welding time, material and passes deposited. Moreover, when the geometry under consideration increases in depth and groove angle, more instances can be built and investigated, exploiting the advantages of the cost function concept, and delivering crucial savings on large scale projects in terms of cost and time planning.

This process can be accelerated if instead of populating all the instances for every sequence of welding parameters, to reject every new incompatible instance when a new layer is added. However, the benefits of investigating the welding sequence from the minimum value of different cost functions, recommends the generation of all the possible instances for every row of array P. Therefore, the series of welding configurations that minimize at the most one of the three parameters (welding time, number of passes, filler material) can be found.

3.5. Formalizing the Deposition of Additional Cap Passes

The need to formalize the input of additional weld cap passes in the path layout model of [24], originates from initial welding trials, where the schematic of the proposed and actual welding solution did not match the expected result. The reasons behind this can be summarized as follows:

- According to the model of the welding torch pose and generated weld pass on [24], the shape of each bead (trapezium/parallelogram) is an approximation of the actual result and the space that will be allocated. However, as the molten weld pool solidifies, gravity and residual stress forces alter the approximated shapes in the cap layer to be more convex, circling the toes of the edges.
- Based on [24], all weld passes are deposited from side to side, and the increased angle of the torch on the first pass of the cap layer relative to the working angle of the root pass leads to overlap a part of the toes of the top surface. Additional passes with the same angle overlap again part of the previous cap passes, resulting in the formation of hollow spaces as can be seen in Figure 11 (a) and (b).

Therefore, the additional cost related to the necessary cap passes is required to be incorporated into the cost function calculation in order for the total minimum solution to be found.

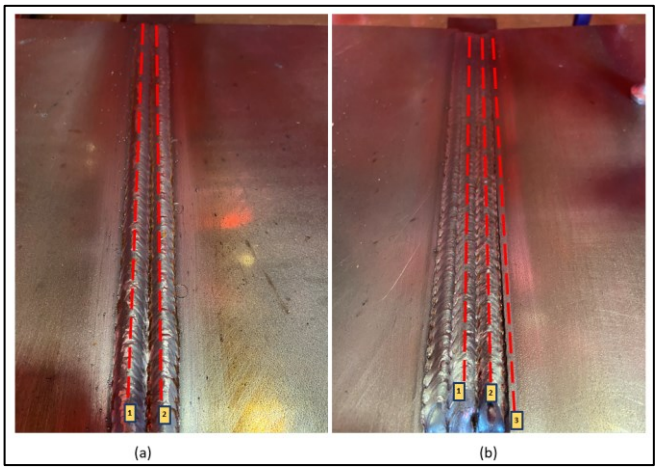

Figure 11. Highlighted formed concave spaces: (a) Between dotted lines 1 and 2 (b) Between dotted lines 1 and 2, 2 and 3

Formalizing these passes depends on the welding parameters of the previous passes in the cap layer. If the total number of weld beads deposited in the cap layer is denoted with letter m, p_m is the offset of the last pass from the middle of the seam and w_m is the weaving width then:

- When $m = 2$, only one additional cap pass is required. The pass is deposited in the middle of the V-groove (zero-offset from root gap) utilizing the same pose as the root pass with wire feed speed 10% less, based on experimental analysis, than what was used for the other passes at the same layer. Moreover, the required weaving width was set to be 3 mm from the experimental trials.
- For the case where $m > 2$ two additional cap passes are required. The first one is deposited between one pass before the last one and the last one with the position offset from the middle of the seam, is given by Eq: 3:7.

$$p_{m+1} = \frac{(p_{m-2} + w_{m-2}) + (p_{m-1} - w_{m-1})}{2} \qquad \textbf{Eq: 3:7}$$

The second pass is deposited with an offset from the middle of the seam based on Eq: 3:8.

$$p_{m+2} = p_{m-1} + w_{m-1} \qquad \textbf{Eq: 3:8}$$

As before the required wire feed speeds for both passes are 10% less than what is assigned in the other passes on the cap layer and the weaving width is 3 mm. Moreover, the angle of the welding torch for the second cap pass was set to be -5º relative to the root pass angle. Consequently, proper fusion is managed with the already deposited pass and the toes of the bevel.

It must be noted that the bevel depth input to the framework should be increased by 1 mm relative to the actual. This action assists in forming a cap layer, where new layers are generated until the total height of the last layer exceeds the groove depth by 1 mm.

The proposed additional cap passes in the welding framework result can be seen schematically with the red dotted lines on the top layers in Figure 12. The selected welding parameters for both cases, were guided from the experimental trials and provided suitable fusion of the two toes of the bevel groove and a clean finish of the cap layer. Formalizing the additional cap passes requirement, allows the generalization of this process in varying V-groove geometries.

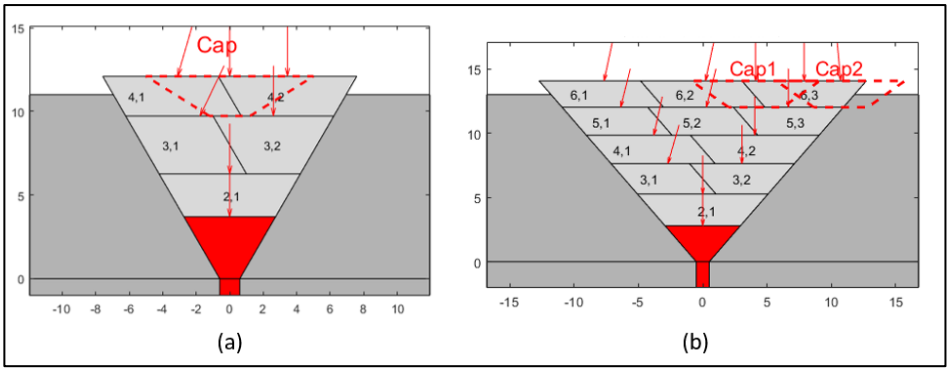

Figure 12. Additional cap passes added to the welding framework solution to compensate between the model and actual welding result: (a) One more cap pass is required in the middle of the seam since the total deposited passes in the top layer were m=2, (b) Two additional cap passes are proposed when m>2 and the deposition position is formalized based on the previous existing passes in the same layer

4. Proof-of-Concept Experimental Verification

4.1. Experimental Setup

A series of experiments were undertaken to prove the feasibility of the proposed welding framework for multi-pass welding, aiming to automate the generation of the robotic motion path, welding parameters allocation and optimisation per layer based on the cost function concept. A 6 DoF articulated robotic welding system was deployed, and two different types of steel of three samples were bevelled under different V-groove geometries as can be seen in Table 7. The robotic setup is shown in Figure 13 and recorded in Table 3.

Table 3. Robotic and welding equipment layout

#	Equipment
1	KUKA KR3-R540
2	Scan-Control 2910-100/BL
3	TBI Weld Torch 22º
4	XIRIS XVC 1000
5	Blackfly PGE50S5C
6	TBI Weld Torch Hose 1.2m
7	Jackle Propuls 400 V wire feeder

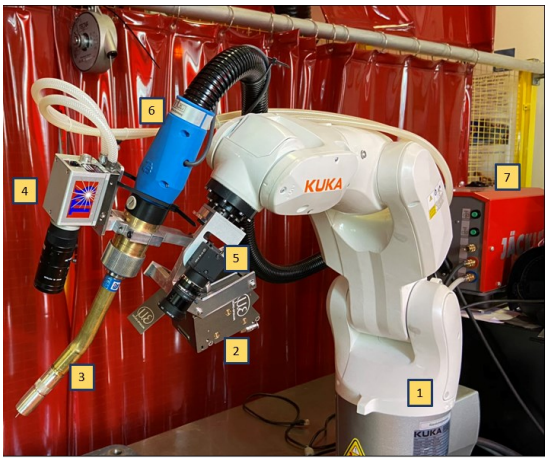

Figure 13. KUKA-KR3 Transformed into a compact welding robot

A laser scanner (2) [28] extracts the geometric characteristics of the V-groove geometry such as the root gap, groove angle, bevel depth, height of root face, length of specimen and height offset of the root pass from the root-face, which are the inputs to the framework. The welding

process was MAG using pulsed current to reduce the welding spatter in absolute wire-feed speed synergic mode [29–31]. Shielding gas ArCO$_2$-(80% Ar + 20% CO$_2$) with a constant flow of 15 l/min and filler solid wire of 1.2 mm diameter was used with characteristics shown in Table 4.

The working angle of the welding torch selected was 65.5º and the wire stick-out was 8.5 mm. A XIRIS high dynamic range weld camera (4) [32] provides visual feedback of the weld pool during welding, and the colour camera (5) [33] locates the weld joint in the scene relative to the reference frame of the welding torch [22]. Robot motion happens through real-time communication provided from the Robot Sensor Interface (RSI) [34] of KUKA at real-time intervals of 4ms. Control of welding dynamics is facilitated from a compact embedded reconfigurable input/output (cRIO 9035) controller of National Instruments (NI) [35], using analogue and digital connections and software developed in LabVIEW environment.

Table 4. Chemical composition of solid wire (%) - (Based on manufacturer certificate)

C	Si	Mn	P	S	Ni	Cr	Mo	Cu	V	Al	N	Ti+Zr
0.081	0.86	1.46	0.011	0.007	0.02	0.04	0.01	0.02	<0.01	<0.01	0.007	0.008

4.2. Welding Parameters Configuration

To determine the deposition coefficient a_H, which is described in Section 3.1, beads with different welding parameters were deposited and the cross-section area of each one was measured using the laser scanner with settings indicated in Table 5. Comparing each cross-section area with the theoretically expected value from Eq:3:2 is shown in Figure 14.

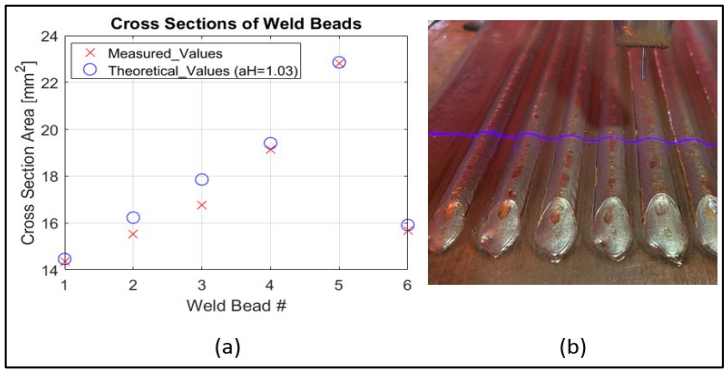

Figure 14. Highlighted cross section of welding beads with different welding parameters: (a) Measured values with laser scanner relative to theoretical values of Eq:3:2, (b) Deposited welding beads (front side-end of weld beads)

Table 5. Laser Scanner 2910-100/BL Inspection setting

Settings Parameter	Value
Exposure Time (ms)	1.5
Number of Profiles (Hz)	105
Saturation (%)	78
Filter Median (taps)	5
Inspection Distance (mm)	140

Obtaining the correct value of a_H is driven from initial trials of welding V-grooves where the proposed schematic solution of the welding joint did not match the volume of the actual welding result. Changing this parameter alters the schematic solution and the proposed number of passes as well. As a result, the constant a_H found to be $a_H = 1.03$. Following this investigation, each of the welding configurations $w_c = [v, u]$ selected for these experiments and used as input to the welding framework are stated in Table 6, sorted in descending order of their cross-section area. The selection of these welding configurations aligns with the industrial partner's WPS for the welding joints provided in Table 7, as well with the purpose to have beads that form a window of varying cross-section area, where in that case covers 14.46 mm^2-17.85 mm^2 . As it is shown in Section 4.3, selecting welding configurations that form a fine window of cross-section areas can lead to different sequences of welding parameters linked to the minimum solution of the cost function for varying V-groove geometries, as well for the same welding geometry and for different cost functions (Table 12).

Table 6. Welding Parameters (n=4) along with theoretical, measured cross-section areas and recorded electrical parameters

Welding Configuration	Robot Speed (mm/s)	Wire Feed Speed (mm/s)	Theoretical Cross Section (mm^2) *	Measured Cross Section (mm^2)	Current (A)	Voltage (Volts)
w_{c1}	5	76.63	17.85	16.77	144	21.9
w_{c2}	5	68.3	15.91	15.69	131	21.3
w_{c3}	5.5	76.63	16.23	15.52	144	21.9
w_{c4}	5.5	68.3	14.46	14.35	131	21.3

* Eq:3:2 calculates the theoretical cross-section area in the welding framework

Moreover, if the number of welding current values increase by two then the wire feed speeds change as well and selecting two additional robot speeds brings the total number of welding configurations to $n + 2 = 6$. Hence, Eq:3:6 storing the number of total permutations, gets the value $(n + 2)^k$ where the size of array P in Figure 9 increases to $(n + 2)^k \times k$ and as a result additional time is required to investigate and build all the different welding instances.

The weaving restriction enforced by parameter delta (δ), was found experimentally to be $\delta = 2$. A condition in weaving reported in [24], was used in the algorithm described in Section 3.2 which compensates the weaving width of the welding torch since the molten weld puddle can fuse with the edges of the groove without the tip of the wire flush with them.

4.3. Experimental Validation and Results

For the experimental verification trials, three different groove geometries and material combinations were selected based on commonly used marine and manufacturing configurations to highlight both the applicability and flexibility of the proposed concept. The geometric characteristics of the welded bevelled joints are shown in, Table 7, along with the minimum value of the used cost function for each sample. The red arrows represent the pose of the welding torch for every weld pass, based on the path layout model presented in [24].

Figure 15 illustrates the 14 deposited weld passes for sample S3 which validates the proposed welding solution in terms of adequately filling the whole groove with the generated welding passes resulting in a cap height above the top surface of average value 0.9 mm. The generated welding parameters produced from the welding framework are stored in Table 8 to Table 10 for S1, S2 and S3 samples, respectively.

Table 7. Highlighted is the proposed solution of the welding framework for each V-groove sample along with the cost function used and geometric properties of the weld joints

Sample #1 (S1)	Sample #2 (S2)	Sample #3 (S3)
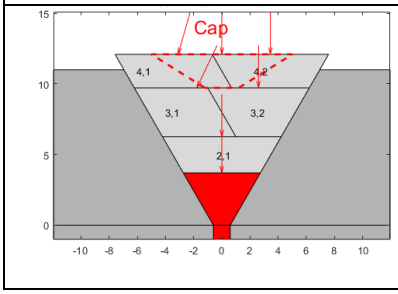	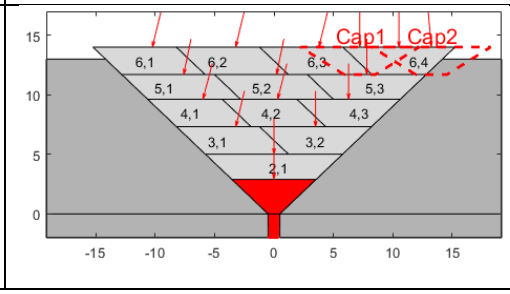	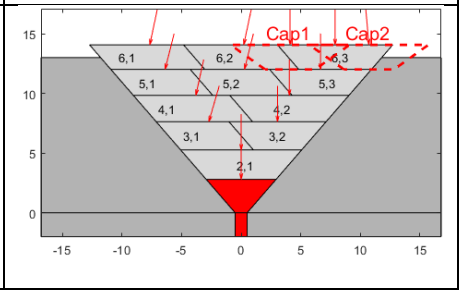
Cost Function		
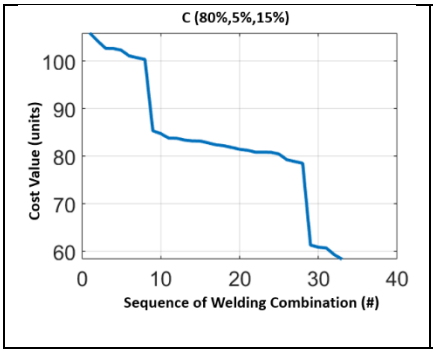	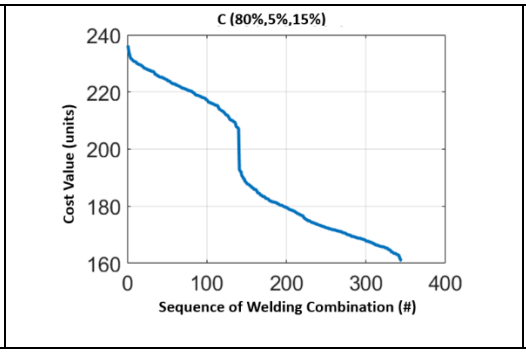	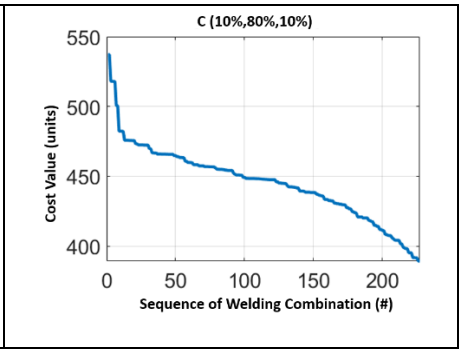
Groove Geometry		
Structural Steel Grade	S-375	S-275	S-275
Root Gap (mm)	1.2	1	1
Welding Wire (mm)	1.2	1.2	1.2
Bevel Depth (mm)	12	13	13
Root-face (mm)	1	2	2

Groove Angle (°)	60	93	82
Root Height Offset (mm)	3.7	2.9	2.8
Length of joint (mm)	300	300	300

509

510

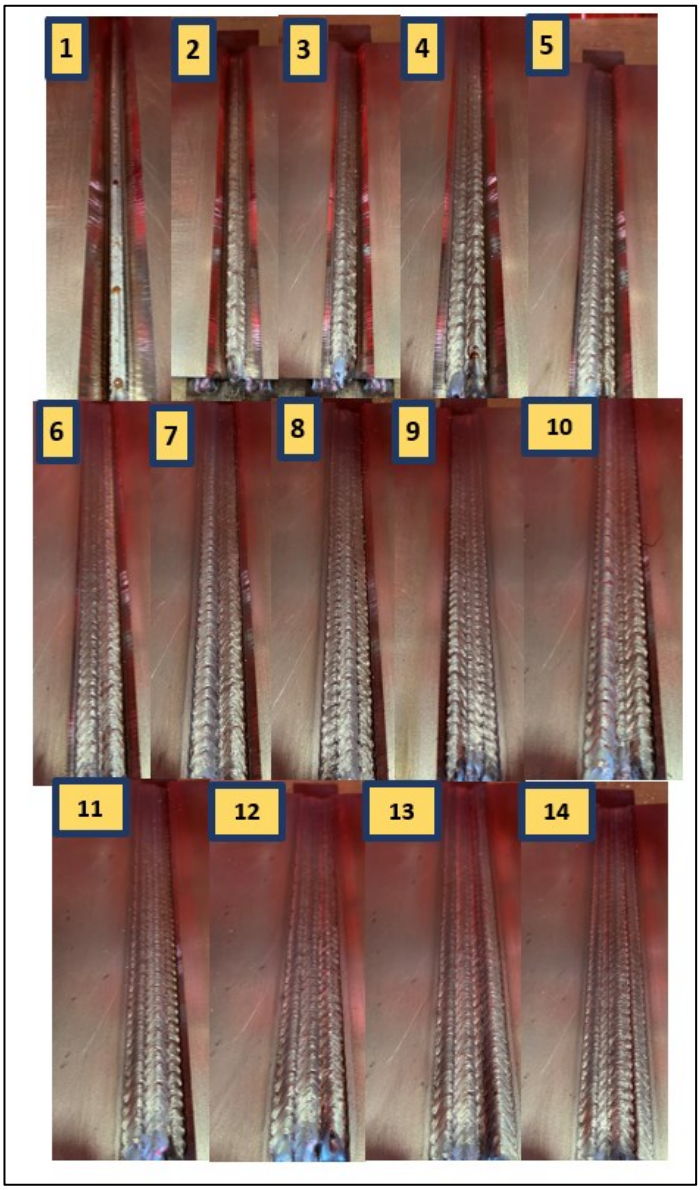

511 **Figure 15. The generated welding sequence for the minimum value of cost function C(10%, 80%, 10%)**
512 **resulted in 14 weld passes for sample S3**

513

514 **Table 8. S1 Generated welding parameters**

Layer Number (#)	Pass Number (#)	Wire Feed	Robot Speed (mm/s)	Offset-middle of the	Height from root-	Angle of	Weaving Width (mm)	Consumable Material (g)	Arc Welding Time (s)

		Speed (mm/s)		seam (mm)	face (mm)	torch (º)			
1	1	60	4.50	0	3.70	0	0.73	32.93	66.66
2	1	83.30	5.50	0	6.26	0	2.21	37.40	54.54
3	1	76.63	5	-1.77	9.72	25.61	1.99	37.85	60
3	2	76.63	5	2.60	9.72	0	1.60	37.85	60
4	1	76.63	5.50	-3.10	12.09	16.02	2.30	34.41	54.54
4	2	76.63	5.50	3.44	12.09	0	2.13	34.41	54.54
4	3	68.96	5.50	0	12.09	0	3	30.97	54.54

515

516 **Table 9. S2 generated welding parameters**

Layer Number (#)	Pass Number (#)	Wire Feed Speed (mm/s)	Robot Speed (mm/s)	Offset-middle of the seam (mm)	Height from root-face (mm)	Angle of torch (º)	Weaving Width (mm)	Consumable Material (g)	Arc Welding Time (s)
1	1	55	5	0	2.90	0	1.55	27.17	60
2	1	93.30	5.50	0	5.01	0	3.78	41.90	54.54
3	1	76.60	5.50	-3.21	7.33	13.77	2.86	34.41	54.54
3	2	76.6	5.50	3.50	7.33	0	2.72	34.31	54.54
4	1	68.30	5.50	-5.98	9.63	14.77	2.50	30.67	54.54
4	2	68.30	5.50	0.30	9.63	14.77	2.50	30.67	54.54
4	3	68.30	5.50	6.29	9.63	0	2.357	30.67	54.54
5	1	76.63	5.50	-7.61	11.70	11.69	3.11	34.41	54.54
5	2	76.63	5.50	0.21	11.70	11.69	3.11	34.41	54.54
5	3	76.63	5.50	7.82	11.70	0	3.00	34.41	54.54
6	1	76.63	5.50	-10.25	14.01	13.72	2.86	34.41	54.54
6	2	76.63	5.50	-3.23	14.01	13.72	2.86	34.41	54.54
6	3	76.63	5.50	3.79	14.01	13.72	2.86	34.41	54.54
6	4	76.63	5.50	10.53	14.01	0	2.73	34.41	54.54
6	5	68.96	5.50	7.236	14.01	0	3	30.97	54.54
6	6	68.96	5.50	13.26	14.01	-5	3	30.97	54.54

517

518 **Table 10. S3 Generated welding parameters**

Layer Number (#)	Pass Number (#)	Wire Feed Speed (mm/s)	Robot Speed (mm/s)	Offset-middle of the seam (mm)	Height from root-face (mm)	Angle of torch (°)	Weaving Width (mm)	Consumable Material (g)	Arc Welding Time (s)
1	1	55	5	0	2.8	0	0.93	27.17	60
2	1	93.30	5.50	0	4.26	0	3.07	41.9	54.54
3	1	68.30	5.50	-2.71	7.63	16.17	2.25	30.67	54.54
3	2	68.30	5.50	3.05	7.63	0	2.08	30.67	54.54
4	1	76.63	5	-3.80	9.84	12.42	3.12	37.85	60
4	2	76.63	5	4.04	9.84	0	3.00	37.85	60
5	1	68.30	5.50	-6.38	12.01	14.24	2.41	30.67	54.54
5	2	68.30	5.50	0.27	12.01	14.24	2.41	30.67	54.54
5	3	68.30	5.50	6.66	12.01	0	2.27	30.67	54.54
6	1	76.63	5.50	-7.67	14.06	11.99	2.94	34.41	54.54
6	2	76.63	5.50	0.21	14.06	11.99	2.94	34.41	54.54
6	3	76.63	5.50	7.88	14.06	0	2.83	34.41	54.54
6	4	68.96	5.50	4.10	14.06	0	3	30.97	54.54
6	5	68.96	5.50	10.72	14.06	-5	3	30.97	54.54

519

520 ### 4.3.1. Ultrasound Inspection for Defects

521 There exists established acceptance standards specific to welds and their final application
522 defining limits related to the presence and size of flaws. These undesirable internal defects can
523 reduce the life span and structural integrity of the weldments [16]. Thus, the integrity of the
524 above welding results are commonly verified through Non-Destructive Testing (NDT) utilizing
525 ultrasound inspection.

526 For that purpose, Phased Array Ultrasonic Testing (PAUT), as the preferred method for
527 inspection of welded samples, is employed to inspect the produced weldments [36]. An
528 ultrasonic probe of 5 MHz with a linear array of 64 elements of 0.5 mm pitch was used to
529 perform sectorial scans. An Ultem wedge of 37.6° was attached to the array and the focal laws
530 were generated to form an S-scan covering a range of 35°-75°. Gain calibration, according to
531 BS EN ISO 17640 was performed, and the reflections from defects compared with the reference

response signal. The calibration is depicted in Figure 17 where two side-drilled holes of ø 2 mm diameter in a 15 mm thick welded section are inspected with the phased array probe. The gain was set to 50 dB, where the signal amplitude indicates 100% of the scale bar.

Following the gain calibration, each produced welded joint was inspected at room temperature along the length of the welding axis. In some positions, lack of root penetration was identified and is reported in Figure 16. No indication for lack of fusion on sidewalls or inter-pass lack of

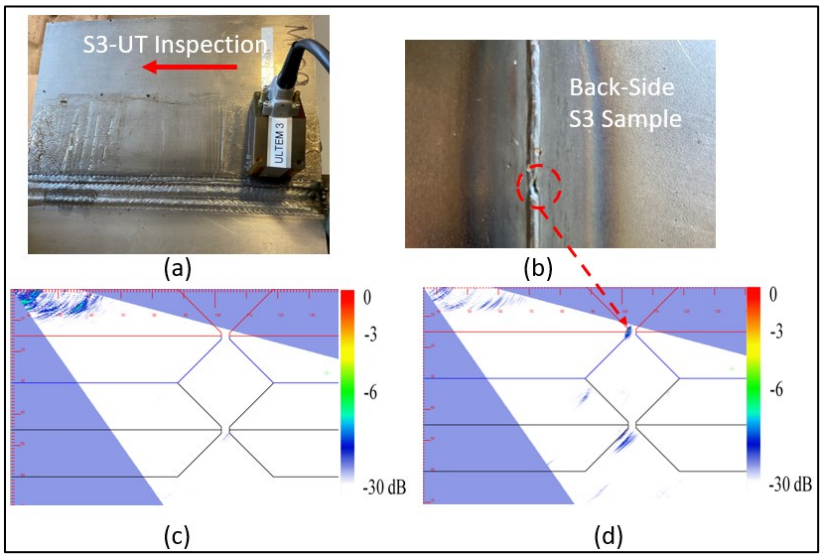

Figure 16. Phased array inspection and indication of lack of root penetration: (a)Sample S3 showing the direction of inspection, (b)Back-side of sample S3 where lack of root penetration exist, indicated by the red circle, (c) Sector scan 35°-75°: where no defects are found,(d) Sector scan 35°-75°: reflection caused from lack of root penetration

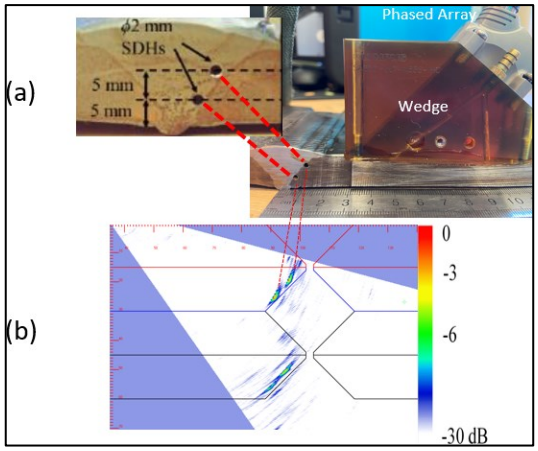

Figure 17. Gain calibration using two side-drilled holes of ø 2 mm for PAUT inspection

fusion was detected across all samples, which can frequently occur in welded joints during manufacturing [37].

Lack of root penetration may have been caused by misalignment fitting of the parent metal plates during joint setup and uneven height of root face caused by bevelling of the weld grooves. As mentioned previously, the welding parameters for root and hot pass are instructed from the operator and are not included in the automation of the proposed welding framework, which is discussed in this paper.

4.3.2. Distortion on the Weldments

Distortion was observed along the vertical direction of welding as shown in Figure 18. The inter-pass temperature was held at 70°C, and clamping was consistent across all samples. Distortion was more severe in samples S2 and S3, where their structural steel grade is lower than S1 and the thickness of the plates is 3 mm higher. Also, on all samples, metal straps were tack welded on both sides to prevent excessive distortion.

Distortion is attributed in the order which the generated welding passes are deposited. The deposition is side to side, always starting from the left of the groove (seen from the front-side of Figure 18) generating increased heat on the left parent plate introducing distortion.

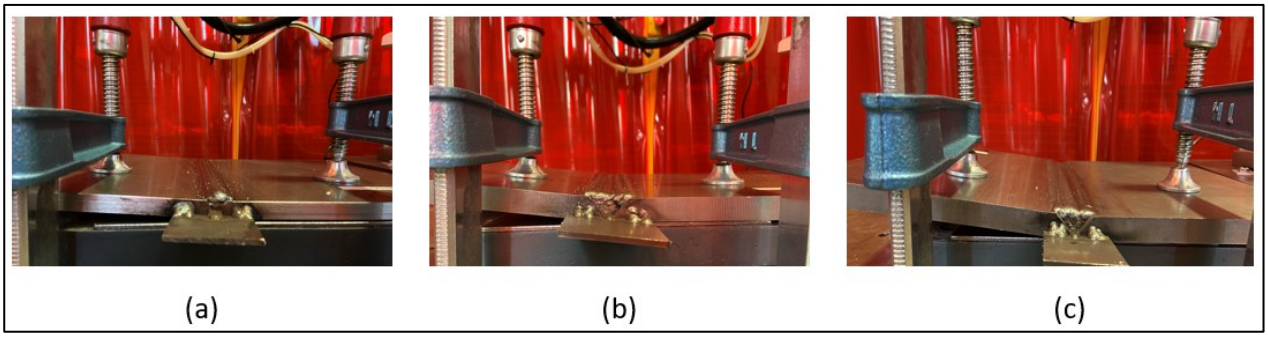

Figure 18. Distortion observed on welded samples: (a) Sample 1-Material S-375 with seven welding passes, (b) Sample 2-Material S-275 with 16 welding passes, (c) Sample 3-Material S-275 with 14 welding passes

Moreover, weaving is required on every welding pass, except the root pass, which increases the heat input as the welding torch spends more time inside the groove.

5. Discussion

5.1. Generated Welding Results and Cost Functions

Three manufactured samples were produced by the proposed welding framework with the cost function concept described in Section 3.4, and presented in this work with welding parameters recorded in Table 8 to Table 10. The samples were welded using the generated welding parameters and visual inspection showed no undercuts or lack of fusion between adjacent passes. This was also validated from the PAUT inspection presented in Section 4.3.1.

The welding parameters utilized to weld each sample, were extracted from the optimum generated instance of the V-groove linked to the minimum value of the assigned cost function. Regarding sample S2, where cost function C(80%, 5%, 15%) was assigned, comparing between its maximum and minimum values, the welding time was decreased by 32.9% and the amount of filler wire by 26.18%. Similar savings are noticed regarding the cost function of sample S3, C(10%, 80%, 10%), where the reduction in welding time and in the amount of filler wire was 28.3% and 27.38% respectively. These reductions are reported in Table 11 for both samples, between maximum and minimum values of each cost function. In addition, from the schematic comparison, the additional amount of filler wire for both samples (purple dotted box), linked to the maximum solution is assigned to the cap pass area, which can be defined as the less efficient solution for the cost function.

Table 11. Comparison between maximum and minimum values of cost function C(80%,5%,15%) and C(10%,80%,10%) respectively for samples S2 and S3 regarding the amount of filler wire and arc time

Sample S2	MAX	MIN	Decrease in %
Amount of filler material (g)	628.18	463.68	26.18
Arc time (s)	1259.1	843.63	32.9
Schematic Solution	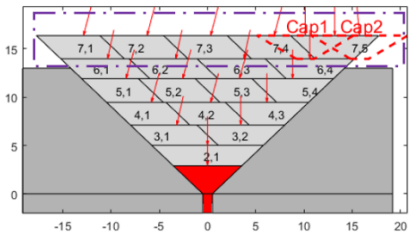	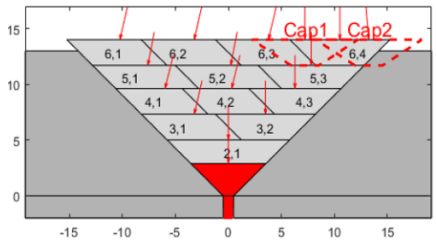	

Sample S3	MAX	MIN	Decrease in %
Amount of filler material (g)	542.97	394.26	27.38
Arc time (s)	1011.8	725.45	28.30

Schematic

Solution

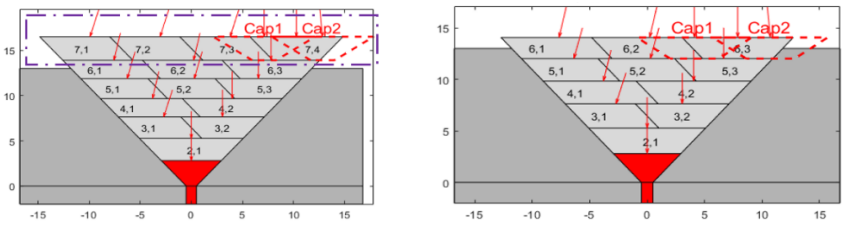

Samples S1 and S2, utilise the same form of the cost function to reflect the difference on the amount of possible unique sequences of welding parameters and the increase in the values that the function receives as the weld groove geometry changes in depth, groove angle and gap offset. As it was expected, sample S2 required two more welding layers and nine welding passes than sample S1. The selection of weighting coefficients for the cost function depends solely on the operator's choice, and different cost functions can be compared only in the degree that the result is driven by the operator's choice of the parameter to minimise at most.

This can be understood better in sample S3 with cost function $C(10\%, 80\%, 10\%)$, which highlights the aim to reduce at most the filler consumable material relative to the other two parameters. Comparing the utilized cost function relative to $C(80\%, 5\%, 15\%)$ for the same sample, the amount of filler wire is reduced by 4.34 grams, but the additional arc welding time is increased by 9.91 seconds since the w_3 is reduced by 5%. The expected outcome which is shown in Table 12, is validated from the reflection of the weighting coefficients in the generated sequence of welding parameters in layers 4 and 5 if the cost function $C(80\%, 5\%, 15\%)$ was deployed instead of $C(10\%, 80\%, 10\%)$.

Table 12. Different generated welding parameters in layers 4 and 5 for sample S3 using cost function C(80%,5%,15%) instead of C(10%,80%,10%)

Layer Number (#)	Pass Number (#)	Wire Feed Speed (mm/s)	Robot Speed (mm/s)	Consumable Material (g)	Arc Welding Time (s)
4	1	76.63	**5/5.50**	**37.85/34.41**	**60/54.54**
4	2	76.63	**5/5.50**	**37.85/34.41**	**60/54.54**
5	1	**68.3/76.63**	5.50	**30.67/34.41**	54.54
5	2	**68.3/76.63**	5.50	**30.67/34.41**	54.54
5	3	**68.3/76.63**	5.50	**30.67/34.41**	54.54

598 Moreover, large variations in the results of different cost functions, for the same geometry, can
599 be achieved when the selected welding parameters w_c stored in vector $\widetilde{W}$ varies a lot in terms
600 of the cross-section area. However, selecting beads with excessive large cross-section area
601 decrease the total welding arc time, whereas the total heat input is increased.

602 The algorithm described in Section 3.2, which is called in every new layer, to determine the
603 number of welding passes has the advantage to adjust the initial welding parameters and adapt
604 in that way to varying V-groove geometries. The manufactured samples did not require this
605 utility, since geometries with groove angles above 95º, tend to require this logic as more passes
606 stack together to reduce the weaving width but conversely the height of the layer increases
607 above the restriction of 5 mm. To better clarify the adaption ability of the framework an
608 example is provided. Considering the V-groove geometry with characteristics as shown in
609 Table 13, using the welding parameters reported in Table 6 and cost function C(80%,5%,15%)
610 it was found that the initial number of layers that can fit according to Section 3.4.1 equals to
611 six. According to Section 3.4.2 investigation for permutations within iterations is performed
612 for seven layers and the total number of permutations based on Eq:3:6 equals to 16,384. It was
613 found that violations on the height and weaving width took place for layers 3,4,5 and 6 and the
614 logic described in Section 3.3 to adapt the given welding parameters was utilized 22,464 times
615 resulting in total additional time of 0.1135 sec. Moreover, the average time spent in this logic
616 when a violation occurred was $5.0537\mathrm{e}-06$ sec and the welding configuration w_c = [5,76.63]
617 had to change to [5.1,73.29] and in other instances to [5.15,71.62], thus two or three iterations
618 of this logic for 22,464 times added the additional time. The reported execution times are
619 extracted from a workstation with an Intel Core i7 @ 2.60 GHz, 16.0 Gb of RAM, Windows
620 10x64 bit architecture.

621 **Table 13. V-groove geometry where violation on height and weaving width occurred in layers 3,4,5 and 6**

Geometric Parameter	Value
Root Gap (mm)	3
Welding Wire (mm)	1.2
Bevel Depth (mm)	15
Root-face (mm)	1
Groove Angle (°)	120
Root Offset (mm)	2.5

622

623 ### *5.2. Performance assessment over the state-of-the-art*

Based on the available information that exists in the relevant works reported in Table 1, an experimental simulation comparison of the performance of the proposed framework is performed.

Regarding [24] and [25] the same groove geometry is used, where in the lateral the wire feed speed used for every welding bead is not reported. This does not allow the calculation of the amount of filler material used. To compare with [24], the same restrictions on the size of the weld bead, weaving width and welding parameters were utilized relative to this method and the cost function C(10%,10%,80%) was assigned to reduce at most the arc welding time. To have a common base of comparison the length of the joint was normalized to 300 mm and the same root pass was used. The results are depicted in Table 14. Following the restrictions on the height and weaving width for every welding layer that exist in [24], one more additional layer and cap pass are added. As explained in Figure 6, this occurs from the investigation for the numbers of layers and passes per layer and the need to find the optimum sequence of welding configurations, by utilizing the same welding parameters as in [24]. As a result, by redistributing the welding parameters and forming the required layers, delivers savings, compared to prompting the user to decide for the number of layers and what are the welding parameters that every layer can get assigned.

Table 14. Quantitative comparison of the proposed welding framework relative to the work reported in [24]

	Layers	Number of Passes	Material (g)	Arc Time (s)
H. Zhang [24]	5	8	1400.49	1815.06
This body of work	6	9	1047.32	1551.33
Difference	+1	+1	-25.22 %	-14.53%

Since in the work reported in [25], the wire feed speed for every pass is omitted and the same groove geometry is used as in [24], the results from the above table are used to compare with the arc time required to weld the whole geometry. It can be seen in Table 15, that the amount of welding passes deposited was 51, thus this method was not efficient to achieve a better arc time than [24] and the proposed work herein.

650 **Table 15. Quantitative comparison of the proposed welding framework relative to the work reported in**
651 **[25]**

	Layers	Number of Passes	Material (g)	Arc Time (s)
S.J. Yan et al [25]	10	51	N/A	3657.45
This body of work	6	9	1047.32	1551.33
Difference	-4	-42	N/A	-57.58%

652

653 The proposed framework is also compared to [23] where a much smaller groove geometry with
654 an angle of 25 ° is utilized than the previous works. The welding parameters for the root-pass
655 from [23] were used. For the filling passes the welding parameters stated in Table 6 were
656 assigned to the vector $\widetilde{W}$, since in [23] the same welding pass is used for all the passes in the
657 different layers. The cost function C(10%,10%,80%) was utilized and the generated results of
658 the welding framework are compared in Table 16.

659 **Table 16. Quantitative comparison of the proposed welding framework relative to the work reported in**
660 **[23]**

	Layers	Number of Passes	Material (g)	Arc Time (s)
T.-Y.Huang et al. [23]	5	7	237.19	432.17
This body of work	6	9	229.69	274.19
Difference	+1	+2	-3.16%	-13.42%

661

662 Regarding [7] and [22], which use the same experimental verification, there are not enough
663 information to validate the characteristics of the utilized V-groove geometry.

664 # 6. Future Work

665 Future work should focus on the full automation of the welding procedure, investigating a
666 suitable methodology for root and hot pass welding parameter allocation based on the gap and
667 root face of the joints. Additionally, the order in which the welding beads are deposited, which
668 revealed distortion, should be investigated, and incorporated to avoid adverse effects on the
669 structural integrity of the weldments. Moreover, effort should be placed on the acceptance
670 flexibility of the framework from irregularities that occur during bevelling and fitting of the
671 parent plates prior to welding. Nonetheless, the procedure described in Section 3.4.3, to find
672 the minimum value of the cost function for all the different weld instances can be optimized

by incorporating other methods, such as random search instead of grid search. This requires the modelling of the probability distribution of the parameters that affect the optimum result and concentrating around this area of search. As a result, this advancement will benefit welding geometries that require numerous welding layers to fill the groove area.

The basis of comparison for the presented welding framework is the current state of the art as depicted in Table 1. In addition, multiple welding trials and characterizations for varying groove geometries will be a key objective of future work.

It must be noted that in this body of work, we do not compare the result with that of a manual welder and what they could achieve, but foresee this as a significant body of future work fully characterizing and quantifying the overall decrease of welding costs through expansion of the cost function minimization approach.

Furthermore, this approach is not limited only in single-sided V-grooves and can be extended to different types of joints such as tee, lap corner and edge where multi-pass welding is required. Therefore, this work can be conceived as the foundation of projecting the multi-pass welding procedure as a real problem in manufacturing through the automation of welding and the benefits it can offer.

7. Conclusion

In this paper, an algorithmic framework for automated off-line robotic multi-pass V-groove weld path planning and sequencing is developed and validated. It can generate robotic welding paths and welding parameters for varying single-sided V-groove geometries, based on the operator's choice to minimize a cost function based on the number of welding passes, welding time and filler wire consumption.

The population of welding passes per layer is driven from the algorithm presented in Sections 3.2 and 3.3, which generates the number of welding beads through the imposed restrictions on maximum weaving and height of every welding pass. The developed work builds on the algorithm in previous work [24] where the user prompts to enter the total number of layers, number of passes and welding parameters. The adaptability of the welding parameters accomplishes the generation of welding passes irrespective of the geometric characteristics of the V-groove geometry. As a result, the robotic weld path planning process is accelerated without the need to re-program and teach the path points in space for the welding torch to follow.

The integrated cost function concept introduces the flexibility in the automation of different welding parameters per layer as happens in manual welding. All the alternative ways that a V-groove geometry can be welded, based on the stored welding configurations on vector $\widetilde{W}$ are investigated, resulting in comparisons and savings between different approaches, always based on the operator's business plan. In this way, planning of resources can be perceived, predicting the overall welding procedure, and instantly deploying robotic welding between different V-groove joints. In practice, the developed system can potentially reduce welding direct costs by minimizing the combination of the number of passes, arc time and filler consumable material through the assigned cost function. For example, in the trial of sample S2, the arc welding time and amount of filler wire were found to be 32.9% and 26.18% lower, respectively, than the worst-case available welding parameter combination. Since an operator does not decide for welding parameters, the cost function always satisfies the optimum result. As a result, a decrease of costs from the worst feasible way to weld the joint is achieved. Nonetheless, indirect costs by utilizing welders in other tasks at the same time and reduced overwork from induced defects can further decrease the manufacturing costs.

Experimental results validate the welding framework utilizing different V-groove geometries of two types of steel grade. The proposed solution for each joint is examined under the actual welding result. Based on the proposed sequence of welding parameters which minimized the allocated cost function along with the respective robotic welding path, fusion of the beads with parent metal is achieved, proving the feasibility of each solution. The need for additional cap passes is reported and formalized to conclude the automated multi-pass robotic welding framework. Moreover, the feasibility of the proposed work is enhanced when the structural integrity of the weldments is assessed using PAUT inspection. Lack of root penetration was reported, which may have be caused by uneven root face of the metal plates from the bevelling of the groove sides and misalignment during fitting. Other defects were not identified, demonstrating an excellent overall fusion of the parent metals under the deposited weld passes.

In summary, this paper introduces and presents a new automated weld parameter and pass deposition sequencing framework, which builds on the current state of the art, that enables automatic planning of multi-pass welding for single-sided V-groove geometries, through minimisation of a user defined novel cost-function for clear commercial and technical benefits.

Acknowledgments

This work was funded under the Maritime, Enterprise, Innovation and Research (MEIR) program and industrial sponsor Babcock International Group PLC.

References

[1] B. Siciliano, O. Khatib, Springer handbook of robotics, Springer, 2016.
[2] R. Timings, Fabrication and Welding Engineering, Routledge, 2008.
[3] R. O'Brien, Welding handbook, vol. 2, American Welding Society. (1991).
[4] R.W. Messler Jr, Principles of welding: processes, physics, chemistry, and metallurgy, John Wiley & Sons, 2008.
[5] What is Gas Metal Arc Welding? (MIG Welding / MAG Welding), (n.d.). https://www.twi-global.com/technical-knowledge/faqs/faq-what-is-mig-mag-welding.aspx (accessed November 10, 2020).
[6] W. Savage, others, Joining of advanced materials, Elsevier, 2013.
[7] C.D. Yang, H.Y. Huang, H.J. Zhang, Y.X. Chen, S.B. Chen, Multi-Pass Route Planning for Thick Plate of Low Alloy High Strength Steel by Double-Sided Double Arc Welding, AMR. 590 (2012) 28–34. https://doi.org/10.4028/www.scientific.net/AMR.590.28.
[8] M.G. Murch, Chapter 2 - Mechanised arc welding process options for pipework fabrications, in: W. Lucas (Ed.), Process Pipe and Tube Welding, Woodhead Publishing, 1991: pp. 21–34. https://doi.org/10.1533/9781845698881.21.
[9] R.M. Stern, A. Berlin, A. Fletcher, K. Hemminki, J. Jarvisalo, J. Peto, International conference on health hazards and biological effects of welding fumes and gases, Int. Arch Occup Environ Heath. 57 (1986) 237–246. https://doi.org/10.1007/BF00405791.
[10] D. Lee, Robots in the shipbuilding industry, Robotics and Computer-Integrated Manufacturing. 30 (2014) 442–450. https://doi.org/10.1016/j.rcim.2014.02.002.
[11] M. Myhr, Industrial new trends: ABB view of the future, in: International Workshop on Industrial Robotics, New Trends and Perspectives (Http://Robotics. Dem. Uc. Pt/Ir99/), Parque Das Nações, Lisbon, 1999.
[12] Y.M. Zhang, R. Kovacevic, L. Li, Adaptive control of full penetration gas tungsten arc welding, IEEE Transactions on Control Systems Technology. 4 (1996) 394–403. https://doi.org/10.1109/87.508887.
[13] C. Doumanidis, Y.-M. Kwak, Multivariable adaptive control of the bead profile geometry in gas metal arc welding with thermal scanning, International Journal of Pressure Vessels and Piping. 79 (2002) 251–262. https://doi.org/10.1016/S0308-0161(02)00024-8.
[14] L. Na, S. Chen, Q. Chen, W. Tao, H. Zhao, S. Chen, Dynamic welding process monitoring based on microphone array technology, Journal of Manufacturing Processes. 64 (2021) 481–492. https://doi.org/10.1016/j.jmapro.2020.12.023.
[15] CEDEFOP, Skill shortages and gaps in European enterprises: Striking a balance between vocational education and training and the labour market, Publications Office Luxembourg, 2015.
[16] W. Fricke, Fatigue analysis of welded joints: state of development, Marine Structures. 16 (2003) 185–200.
[17] CaB System 300S/300M, (n.d.). https://www.esab.co.uk/gb/en/ (accessed November 24, 2020).
[18] Making the Cut with KUKA Robotics Corporation at FABTECH 2015 Chicago, (2015). https://www.businesswire.com/news/home/20151106005066/en/Making-the-Cut-with-KUKA-Robotics-Corporation-at-FABTECH-2015-Chicago (accessed November 24, 2020).

[19] T.S. Hong, M. Ghobakhloo, W. Khaksar, 6.04 - Robotic Welding Technology, in: S. Hashmi, G.F. Batalha, C.J. Van Tyne, B. Yilbas (Eds.), Comprehensive Materials Processing, Elsevier, Oxford, 2014: pp. 77–99. https://doi.org/10.1016/B978-0-08-096532-1.00604-X.
[20] J.N. Pires, A. Loureiro, G. Bölmsjo, eds., Robotic Welding: System Issues, in: Welding Robots: Technology, System Issues and Applications, Springer London, London, 2006: pp. 105–145. https://doi.org/10.1007/1-84628-191-1_4.
[21] K. Xue, Z. Wang, J. Shen, S. Hu, Y. Zhen, J. Liu, D. Wu, H. Yang, Robotic seam tracking system based on vision sensing and human-machine interaction for multi-pass MAG welding, Journal of Manufacturing Processes. (2020). https://doi.org/10.1016/j.jmapro.2020.02.026.
[22] C. Yang, Z. Ye, Y. Chen, J. Zhong, S. Chen, Multi-pass path planning for thick plate by DSAW based on vision sensor, Sensor Review. 34 (2014) 416–423. https://doi.org/10.1108/SR-04-2013-649.
[23] T.-Y. Huang, L.-W. Fan, Y.-N. Bao, H. Shi, K. Zhang, Multi-pass Route Planning for Thick Steel Plate Using Laser Welding with Filler Wire, in: T.-J. Tarn, S.-B. Chen, X.-Q. Chen (Eds.), Robotic Welding, Intelligence and Automation, Springer International Publishing, Cham, 2015: pp. 551–560. https://doi.org/10.1007/978-3-319-18997-0_47.
[24] H. Zhang, H. Lu, C. Cai, S. Chen, Robot Path Planning in Multi-pass Weaving Welding for Thick Plates, in: T.-J. Tarn, S.-B. Chen, G. Fang (Eds.), Robotic Welding, Intelligence and Automation, Springer, Berlin, Heidelberg, 2011: pp. 351–359. https://doi.org/10.1007/978-3-642-19959-2_43.
[25] S.J. Yan, S.K. Ong, A.Y.C. Nee, Optimal Pass Planning for Robotic Welding of Large-dimension Joints with Deep Grooves, Procedia CIRP. 56 (2016) 188–192. https://doi.org/10.1016/j.procir.2016.10.052.
[26] T.-L. Teng, P.-H. Chang, W.-C. Tseng, Effect of welding sequences on residual stresses, Computers & Structures. 81 (2003) 273–286. https://doi.org/10.1016/S0045-7949(02)00447-9.
[27] C. Heinze, C. Schwenk, M. Rethmeier, Numerical calculation of residual stress development of multi-pass gas metal arc welding, Journal of Constructional Steel Research. 72 (2012) 12–19. https://doi.org/10.1016/j.jcsr.2011.08.011.
[28] Reference Manual-Scan Control Laser Scanner 2910-100/BL, (n.d.). https://www.micro-epsilon.co.uk/download/manuals/man--scanCONTROL-29xx--en.pdf (accessed November 12, 2020).
[29] T. Era, T. Ueyama, Spatter reduction in GMAW by current waveform control, Welding International. 21 (2007) 496–501. https://doi.org/10.1080/09507110701579647.
[30] S.H. Lee, J.S. Kim, B.Y. Lee, S.Y. Lee, The Effect of External Electromagnetic Force in Gas Metal Arc Welding on the Transfer Mode, Key Engineering Materials. 297–300 (2005) 2825–2830. https://doi.org/10.4028/www.scientific.net/KEM.297-300.2825.
[31] Z. Wang, D. Jiang, J. Wu, M. Xu, A review on high-frequency pulsed arc welding, Journal of Manufacturing Processes. 60 (2020) 503–519. https://doi.org/10.1016/j.jmapro.2020.10.054.
[32] Xiris resources, Xiris Automation Inc. (n.d.). https://www.xiris.com/resources/ (accessed November 12, 2020).
[33] Blackfly S Documentation, (n.d.). http://softwareservices.flir.com/BFS-PGE-50S5/latest/Model/Readme.html (accessed November 12, 2020).
[34] KUKA R.S.I. 4.0, (n.d.). https://xpert.kuka.com/ID/AR16559 (accessed November 12, 2020).
[35] National Instruments, Manual cRIO 9035, (n.d.). https://www.ni.com/pdf/manuals/376935e_03.pdf (accessed November 12, 2020).

[36] A. Erhard, G. Schenk, Th. Hauser, U. Völz, New applications using phased array techniques, Nuclear Engineering and Design. 206 (2001) 325–336. https://doi.org/10.1016/S0029-5493(00)00419-2.
[37] N.T. Burgess, Quality Assurance of Welded Construction., Routledge, Hoboken, 1989. http://public.ebookcentral.proquest.com/choice/publicfullrecord.aspx?p=242049 (accessed October 26, 2020).